Tailoring the phase-matching function for ultrashort pulse characterization by spectral shearing interferometry

S.-P. Gorza,[1,*] A. S. Radunsky,[1,2] P. Wasylczyk,[1,3] and I. A. Walmsley[1]

[1]*Clarendon Laboratory, University of Oxford, Parks Road, Oxford, OX1 3PU, UK*
[2]*Institute of Optics, University of Rochester, Rochester, New York 14627, USA*
[3]*Institute of Experimental Physics, University of Warsaw, ul. Hoża 69, 00-681 Warsaw, Poland*
[*]*Corresponding author: sgorza@ulb.ac.be*

Received December 8, 2006; revised April 22, 2007; accepted April 25, 2007;
posted May 14, 2007 (Doc. ID 77898); published July 30, 2007

Sum-frequency generation using spectrally asymmetric type II phase matching enables significant simplifications in spectral shearing interferometry as applied for ultrashort optical pulse measurements. We present analytical and numerical models of broadband sum-frequency wave mixing essential to understand the underlying effects. We discuss spectral and temporal limits of the method together with various aspects of experimental implementation: optimization of the retrieval algorithm, calibration procedures, and extension to different spectral regions of particular interest with other crystals. © 2007 Optical Society of America

OCIS codes: 320.7160, 320.7100, 190.4360.

1. INTRODUCTION

It is the unprecedented electric field intensities generated and/or the duration of the pulses itself that have established ultrashort optical pulses as an important tool in physics, chemistry, biology, and medicine. In either case, the ability to characterize the pulse's electric field in time, or equivalently in frequency, is a route toward new experiments as well as the improvement of the range and the reliability of the already well-established ultrafast techniques and technologies. With commercial, turn-key operated lasers routinely generating sub-10 fs pulses, the quest for sensitive, simple, and trustworthy techniques of pulse measurement incarnated in compact devices attracts many leading groups worldwide.

Since the only available nonstationary filters with femtosecond time resolution are based on nonlinear frequency conversion (most often in birefringent nonlinear crystals), all the current pulse characterization techniques rely on such processes [1]. An important step forward was the realization that by the proper phase-matching management of these crystals, the pulse measurement can be significantly simplified [2]. Subsequently, a new range of techniques emerged, among them GRENOUILLE, a spectrographic method based on frequency-resolved optical gating (FROG) redesigned with thick crystal and no spectrometer [3] and the single shot sonogram [4], utilizing a similar effect.

Only recently was it demonstrated that the spectral shearing interferometry may also benefit from a better understanding of the phase-matching with broadband fields and ARAIGNEE (another ridiculous acronym for interferometic geometrically simplified noniterative *E*-field extraction) saw its first light [5]. The sum-frequency (SF) generation in a properly chosen nonlinear crystal is itself used to generate frequency sheared pulse replicas [6]. Thus a fundamental requirement for spectral phase interferometry for direct electric field extraction (SPIDER) [7] can be realized without a separate ancillary pulse leading to a significant simplification of the technique.

In this paper we present a number of theoretical and practical issues pertinent to ARAIGNEE: we analyze broadband type II SF generation in the phase-matching picture as well as in the framework of the interacting pulsed fields; we discuss the pulse retrieval procedure including corrections accounting for nonperfect group velocity matching and group velocity dispersion and present further experimental details of the technique. We have shown that ARAIGNEE may be implemented in very simple, compact, and sensitive apparatuses [8] (see also Fig. 2). Still, for reliable ultrashort pulse measurements over broad bandwidths as well as defining the limits of the technique, a better understanding of the upconversion process is essential. Several numerical simulations of the SF generation are presented both to validate our analytical results and to predict the spectral tunability range and the bandwidth limitations of ARAIGNEE. Three widely used nonlinear crystals are investigated: potassium dihydrogen phosphate (KDP), potassium titanyl phosphate (KTP) and β-barium borate (BBO). These crystals are suitable to characterize with high accuracy ultrashort pulses in the spectral ranges 740–900 nm, 1000–1300 nm and 1200–1600 nm, respectively, and for pulse duration between 50 and 600 fs. Experimental results are presented and discussed for a number of pulses under study, in particular those with parameters at the theoretical limits of the measurement device performance.

2. PHASE-MATCHING ENGINEERING

The underlying principle of spectral shearing interferometry is to resort to a spectrally shifted (sheared) replica of the test pulse to measure itself. In conventional SPIDER, for pulses above 20 fs, the spectral shear is produced by upconverting two pulse replicas with different quasi-monochromatic time slices of a highly chirped ancillary pulse [7]. For ultrashort pulses of 10 fs or less, in order to not alter the unknown pulse before it arrives at the nonlinear crystal, a single test pulse upconverts with two highly chirped ancillary pulses [9–11]. What is therefore essential for either configuration is a nonlinear process that can mix a broadband test pulse with a quasimonochromatic (narrowband) wave, or ancillary pulse, hereafter labeled the ancilla. Since the ancilla is typically prepared outside the nonlinear crystal, the only requirement on the crystal is that its phase-matching function (PMF), which links the upconverted pulse to the input pulse, should not introduce any phase distortion. A thin nonlinear crystal, typically in the range of a few tens of micrometers, is used to achieve a sufficiently large bandwidth.

In ARAIGNEE the crystal is chosen so that the narrowband ancilla is selected directly from the test pulse by the PMF of the nonlinear crystal itself (see Fig. 1).

In the frequency domain, this can be described as follows: Let us represent the complex amplitude of the input test pulse, $E(t)$ by a Fourier transformation, $\tilde{E}(\omega) = \int E(t)\exp(i\omega t)\mathrm{d}t$. We are interested in generating a spectrally shifted replica of the input: $\tilde{E}(\omega) \rightarrow \tilde{E}(\omega - \Omega)$, where Ω is the spectral shear. Considering an $\chi^{(2)}$ nonlinear crystal, we can approximate the SF signal, $\tilde{E}_s(\omega)$ for two arbitrary input fields, $\tilde{E}_1(\omega_1)$ and $\tilde{E}_2(\omega_2)$ as [12]:

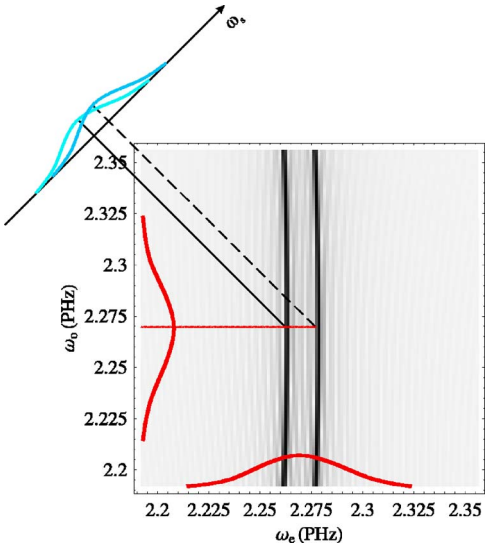

Fig. 1. (Color online) Absolute magnitudes of the collinear type II PMF $|\Phi|^2$ of a 20 mm thick KDP crystal for two values of the propagation angle (0.5° apart), plotted as a function of frequency for ordinary ω_o and extraordinary ω_e input polarization components (black indicating perfect phase-matching). The SF signals are drawn on the diagonal axis, $\omega_s = \omega_e + \omega_o$, illustrating the shear between the outputs due to the specific PMF shape, which allows all the frequency content of one of the input fields to mix with a single frequency component of the other one.

$$\tilde{E}_s(\omega) \propto \int\int \delta(\omega_1 + \omega_2 - \omega)\tilde{E}_1(\omega_1)\tilde{E}_2(\omega_2)\Phi(\omega_1, \omega_2)\mathrm{d}\omega_1\mathrm{d}\omega_2$$

$$= \int \tilde{E}_1(\omega - \omega_2)\tilde{E}_2(\omega_2)\Phi(\omega - \omega_2, \omega_2)\mathrm{d}\omega_2, \quad (1)$$

where δ denotes the delta function and the PMF of the interaction in the crystal is represented by

$$\Phi(\omega_1, \omega_2) = \sin(T)/T \times \exp(iT), \quad (2)$$

where $T(\omega_1, \omega_2) = [k_1(\omega_1) + k_2(\omega_2) - k_s(\omega_1 + \omega_2)]L/2$, L is the interaction length and k_j is the propagation constant of the $j = \{1, 2, s\}$ field.

For a conventional SPIDER device that uses a sufficiently thin crystal, the PMF can be approximated as $\Phi(\omega_1, \omega_2) \simeq 1$ over the pulse bandwidth, and the SF generation process described by Eq. (1) is then equivalent to a convolution of the two fundamental fields:

$$\tilde{E}_s(\omega) = \tilde{E}_1(\omega) * \tilde{E}_2(\omega) = \int \tilde{E}_1(\omega - \omega_2)\tilde{E}_2(\omega_2)\mathrm{d}\omega_2. \quad (3)$$

Therefore, if one of the fundamental beams is a quasi-monochromatic ancilla and can be approximated by a delta function, $\tilde{E}_1 \simeq \delta(\omega - \Omega)$, then Eq. (3) represents an exact spectrally shifted replica of the broadband input pulse: $\tilde{E}_s(\omega) = \tilde{E}_2(\omega - \Omega)$.

To visualize the main idea of ARAIGNEE, we must return to Eq. (1) and consider the case when the PMF $\Phi(\omega_1, \omega_2)$ can be written as a direct product of two one-dimensional (1D) functions, $\Phi(\omega_1, \omega_2) = \Phi_1(\omega_1) \times \Phi_2(\omega_2)$. This factorization of the PMF means that the SF field of Eq. (1) is now also a convolution of the two inputs, each modified by its respective PMF component:

$$\tilde{E}_s(\omega) = [\Phi_1(\omega)\tilde{E}_1(\omega)] * [\Phi_2(\omega)\tilde{E}_2(\omega)]. \quad (4)$$

As a result, if we can arrange for the factorization to be of the form $\Phi_1(\omega) \times \Phi_2(\omega) = \delta(\omega - \Omega) \times 1$, the output pulse is still a replica of one of the input pulses $[\tilde{E}_s(\omega) = \tilde{E}_2(\omega - \Omega)]$ with the only requirement on the other one $(\tilde{E}_1)$ being that it contains the frequency Ω.

Figure 1 shows such a situation, where the PMF magnitude $(|\Phi|^2)$ has been plotted for optical fields traveling at two angles tilted by ±0.25° away from the normal to the surface of a 2 cm long type II KDP crystal cut for second harmonic generation at 830 nm ($\theta = 68°$). The particular combination of the crystal dispersion, the cut angle, and the wavelength range produces a nearly vertical PMF that is simultaneously very broad along the ordinary axis and very narrow along the extraordinary axis. Such a highly asymmetric PMF shape is the result of a group velocity match between the *o*-fundamental input and the *e*-upconverted output field and a group velocity mismatch between the *e*-fundamental and the *e*-upconverted fields. Because of this specific PMF, the entire bandwidth of an *o*-pulse, with the spectrum located in the 830 nm region, may convolve with a quasi-monochromatic portion of the *e*-pulse spectrum as selected by the PMF. The angle of propagation relative to the crystal optic axis determines the wavelength of the monochromatic slice of the *e*-wave bandwidth that upconverts with the entire *o*-wave band-

width. Thus, if two copies of a pulse are directed into the crystal, altering their respective propagation angles produces the spectral shift between the upconverted outputs required for the spectral shearing interferometry.

One of the recent realizations of the ARAIGNEE apparatus is presented schematically in Fig. 2. The two pulse replicas are generated by sending the input beam onto a mirror pair, and the relative angle between them allows the replicas to propagate in the nonlinear crystal (KDP) with a slightly different angle. Apparently, the setup requires only a few optical elements, enabling us to build a very compact apparatus. It is worth mentioning that in ARAIGNEE the only degree of freedom in the SF generation is the phase-matching angle, which is the horizontal tilt of the nonlinear crystal, since the spatial and the temporal overlap of all the pulses is automatically met.

3. ANALYTICAL DESCRIPTION OF THE SUM-FREQUENCY GENERATION

The simple picture developed in Section 2 is not sufficient to explore the entire potential of ARAIGNEE. Indeed, since we are dealing with the nonlinear interaction of pulses, not only the magnitude of the PMF as depicted in Fig. 1 but also its phase have to be taken into account. We have therefore developed a more comprehensive wave mixing model.

We consider the type II collinear interaction of two fundamental pulses R_o and R_e, respectively, *o*- and *e*-polarized, and the upconverted pulse B generated by SF in a dispersive dielectric medium with $\chi^{(2)}$ nonlinear susceptibility (see Fig. 3). Assuming the complex amplitude envelopes R_o, R_e, and B to be slowly varying, we derive from Maxwell's equations the system of three nonlinear equations coupled parametrically through the components $\chi^{(2)}_{ijk}$ of the nonlinear susceptibility tensor [13]:

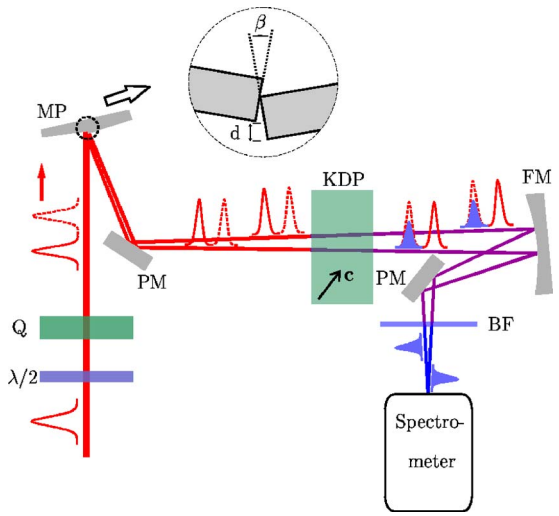

Fig. 2. (Color online) Schematic of the ARAIGNEE device. λ/2, half-wave plate; Q, quartz plate; MP, mutually tilted (by β) and longitudinally shifted (by d) mirror pair; PM, pick-off mirror; FM, focusing mirror; BF, blue filter; KDP, nonlinear crystal. Dotted curves depict ordinary pulses and solid curves, extraordinary pulses.

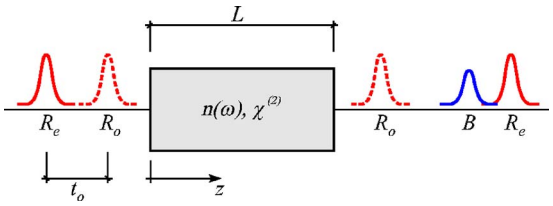

Fig. 3. (Color online) Upconversion in a type II nonlinear crystal. $R_{o,e}$ are the *o*- and *e*-polarized test pulses, respectively, and B is the sum frequency pulse. t_0 is the predelay between the two fundamental test pulses and L is the crystal thickness.

$$
\begin{aligned}
i\partial_z R_o(t,z) + i\Delta k'_{br_o}\partial_t R_o - \frac{k''_{r_o}}{2}\partial_{tt}R_o &= -\Gamma_{r_o}R_e^* B\exp(-i\Delta kz),\\
i\partial_z R_e(t,z) + i\Delta k'_{br_e}\partial_t R_e - \frac{k''_{r_e}}{2}\partial_{tt}R_e &= -\Gamma_{r_e}R_o^* B\exp(-i\Delta kz),\\
i\partial_z B(t,z) - \frac{k''_b}{2}\partial_{tt}B &= -\Gamma_b R_o R_e\exp(i\Delta kz),
\end{aligned}
\tag{5}
$$

where diffraction and spatial walk-off have been neglected. In these equations, z is the propagation distance and t the time in a reference frame traveling at the SF group velocity (k'^{-1}_b) at the frequency $\omega_b=\omega_{r_o}+\omega_{r_e}$ where ω_{r_o} and ω_{r_e} are the carrier frequencies of the two fundamental waves; $\Gamma_l=(\omega_l^2/2k_lc^2)\chi_l^{(2)}$ $(l=r_o,r_e,b)$ is the nonlinear coupling coefficient. $\Delta k=k_{r_o}+k_{r_e}-k_b$ is the wave vector mismatch, $\Delta k'_{bj}=k'_j-k'_b$ the group velocity mismatch while $k'_l=\partial k_l/\partial_{\omega_l}$ and $k''_l=\partial^2 k_l/\partial^2_{\omega_l}$ are the inverse of the group velocities and the group velocity dispersions (GVD), respectively.

A. Dispersionless Medium

Let us first consider a dispersionless medium. If the nonlinear interaction is weak, the fundamental waves propagate undistorted in the medium and the system (5) can be reduced to a single equation for the SF wave:

$$
\frac{\partial}{\partial z}B(t,z) = i\Gamma_b R_o(t-\Delta k'_{br_o}z)R_e(t-\Delta k'_{br_e}z-t_0)\exp(i\Delta kz),
\tag{6}
$$

where t_0 is the predelay between the two fundamental pulses at $z=0$. In a negative (positive) crystal, the *e*-polarized fundamental pulse is faster (slower) than the *o*-polarized one. Therefore t_0 has to be positive (negative) as the two pulses cross each other in the nonlinear medium.

The complex envelope of the SF wave at the output of the crystal of length L is formally obtained by integrating the right-hand side of Eq. (6) from $z=0$ to $z=L$:

$$
B(t,L) = i\Gamma_b\int_0^L R_o(t-\Delta k'_{br_o}z)R_e(t-\Delta k'_{br_e}z-t_0)\exp(i\Delta kz)\mathrm{d}z.
\tag{7}
$$

For the sake of simplicity, we particularize our discussion to negative crystals, but it can straightforwardly be

applied to positive crystals. Assuming that the fastest pulse (R_e) walks completely through the slowest on (R_o) and does not overlap with R_o either before or after the crystal, we can extend the integration boundaries of Eq. (7) to $\pm\infty$. In this experiment, this condition can be achieved by choosing a predelay t_0 greater than the time support (ΔT) of the test pulse, and a crystal length such that $L > (\Delta T + |t_0|)/|\Delta k'_{r_e r_o}|$.

Replacing R_o by its frequency representation in the spectral domain:

$$R_o(t - \Delta k'_{br_o} z) = \frac{1}{2\pi}\int_{-\infty}^{\infty} \tilde{R}_o(\omega)\exp(i\Delta k'_{br_o} z\omega)\exp(-i\omega t)\mathrm{d}\omega, \tag{8}$$

Eq. (7) reads

$$B(t,L) = \frac{i\Gamma_b}{2\pi}\int_{-\infty}^{\infty} \tilde{R}_o(\omega)\exp(-i\omega t)\int_{-\infty}^{\infty} R_e(t - \Delta k'_{br_e} z - t_0) \times \exp[i(\Delta k + \Delta k'_{br_o}\omega)z]\mathrm{d}z\mathrm{d}\omega. \tag{9}$$

To perform the integration over z, the following variable change, $\tau = t - \Delta k'_{br_e} z - t_0$, is introduced and Eq. (9) becomes

$$B(t,L) = \frac{-i\Gamma_b}{2\pi\Delta k'_{br_e}}\int_{-\infty}^{\infty} \tilde{R}_o(\omega)\exp(-i\omega t)\int_{-\infty}^{\infty} R_e(\tau) \times \exp\left[i\frac{\Delta k + \Delta k'_{br_o}\omega}{\Delta k'_{br_e}}(t - \tau - t_0)\right]\mathrm{d}\tau\mathrm{d}\omega. \tag{10}$$

The integration over τ gives

$$\int_{-\infty}^{\infty} R_e(\tau)\exp\left(-i\frac{\Delta k + \Delta k'_{br_o}\omega}{\Delta k'_{br_e}}\tau\right)\mathrm{d}\tau = \tilde{R}_e\left(-\frac{\Delta k + \Delta k'_{br_o}\omega}{\Delta k'_{br_e}}\right), \tag{11}$$

and to solve Eq. (10), Eq. (11) is expanded in a series around $\omega = 0$:

$$\tilde{R}_e\left(-\frac{\Delta k + \Delta k'_{br_o}\omega}{\Delta k'_{br_e}}\right) = \tilde{R}_e\left(-\frac{\Delta k}{\Delta k'_{br_e}}\right) - \frac{\Delta k'_{br_o}}{\Delta k'_{br_e}}\omega\tilde{R}'_e\left(-\frac{\Delta k}{\Delta k'_{br_e}}\right) + O(\omega^2), \tag{12}$$

where $'$ denotes derivation with respect to the argument of R_e.

In a crystal with a nearly vertical PM function as in Fig. 1, there is a group velocity mismatch between the two fundamental pulses (i.e., $\Delta k'_{r_o r_e} \neq 0$) and at the same time a group velocity match between the o-fundamental and the SF pulses (i.e., $\Delta k'_{br_o} \approx 0$). As a result, $\Delta k'_{br_o}/\Delta k'_{br_e} \ll 1$ and only the first term of the right-hand side of Eq. (12) is kept. Therefore Eq. (10) is approximated by

$$B(t,L) \approx \frac{-i\Gamma_b}{2\pi\Delta k'_{br_e}}\tilde{R}_e\left(-\frac{\Delta k}{\Delta k'_{br_e}}\right)\exp\left[i\frac{\Delta k}{\Delta k'_{br_e}}(t - t_0)\right] \times \int_{-\infty}^{\infty} \tilde{R}_o(\omega)\exp(-i\omega t)\exp\left[i\frac{\Delta k'_{br_o}}{\Delta k'_{br_e}}(t - t_0)\omega\right]\mathrm{d}\omega. \tag{13}$$

Fourier transforming back $\tilde{R}_o$, the SF pulse at the output of the crystal is

$$B(t,L) = \frac{-i\Gamma_b}{\Delta k'_{br_e}}\tilde{R}_e\left(-\frac{\Delta k}{\Delta k'_{br_e}}\right)\exp\left[i\frac{\Delta k}{\Delta k'_{br_e}}(t - t_0)\right] \times R_o\left(t\left[1 - \frac{\Delta k'_{br_o}}{\Delta k'_{br_e}}\right] + t_0\frac{\Delta k'_{br_o}}{\Delta k'_{br_e}}\right). \tag{14}$$

Equation (14) shows that the SF pulse B is a replica of the R_o pulse, i.e., the fundamental pulse that travels in the nonlinear crystal with approximately the same group velocity as the SF pulse. However, this replica is a time-scaled copy of R_o with the scaling factor s:

$$s = 1 - \frac{\Delta k'_{br_o}}{\Delta k'_{br_e}}. \tag{15}$$

The scaling factor is thus equal to 1 when the group velocities of B and R_o are perfectly matched. The expression (15) is in agreement with the results reported in [14]. However our theoretical analysis shows that this result holds even if the fundamental wave R_e is not a δ function, as long as the high order terms in Eq. (12) can be neglected.

The spectrum of the replica is centered around the frequency $\omega_b = \omega_{r_o} + \omega_{r_e} - \Delta k/\Delta k'_{br_e}$ and its amplitude is proportional to the spectral amplitude $\tilde{R}_e$ at the frequency $\omega = -\Delta k/\Delta k'_{br_e}$. We can thus interpret the SF process as a waveform transfer from the o-wave to the SF-wave by mixing a quasi-monochromatic slice of the spectrum of the e-wave with the whole spectrum of the o-wave. The actual frequency of the quasi-monochromatic slice is defined by the PMF: If we take into account only the lowest order terms in the power expansion of the wave vectors in the vicinity of the center frequency [15], then the phase mismatch is

$$\Delta k + k'_{r_o}(\omega_1 - \omega_{r_o}) + k'_{re}(\omega_2 - \omega_{r_e}) - k'_b(\omega_3 - \omega_b) = 0. \tag{16}$$

Taking $\omega_1 = \omega_{r_o}$ (the central frequency of the spectrum that is entirely upconverted) and $\omega_2 = \omega_{r_e} + \Delta\omega$, hence $\omega_3 = \omega_{r_o} + \omega_{r_e} + \Delta\omega$ and Eq. (16) leads to

$$\Delta\omega = -\Delta k/\Delta k'_{br_e}. \tag{17}$$

This result is consistent with the simplified picture of the SF generation discussed in Section 2 on the basis of the PMF of continuous waves [6].

Eventually, from Eq. (14) it can be seen that, in the reference frame traveling at the group velocity k'^{-1}_b, the SF pulse is temporally shifted by

$$\Delta t = t_0 \Delta k'_{br_o} / \Delta k'_{r_o r_e}. \quad (18)$$

This latter result has been previously derived in [14] from the assumption that the SF pulse is generated in the crystal at the location where the two fundamental pulses meet in the crystal. Here we derive the result from first principles. The predicted temporal shift agrees well with experimental measurements.

To verify our analytical results, we have numerically simulated the propagation of the pulses in the nonlinear crystal by solving the system (5) with a standard beam propagating method [16]. The solid curves in Fig. 4 show the temporal amplitude and phase of the SF pulse at two different locations in the nonlinear crystal. The initial condition corresponds to two identical Gaussian chirped input pulses for the two fundamental waves: $R_o(t)=\exp[-(t/T)^2]\times\exp[i0.5(t/T)^2]$ and $R_e(t)=0.7R_o(t-t_0)$ where $t_0=4.3T$ such that the two pulses do not overlap in $z=0$. Moreover we have assumed a perfect group velocity match between the *o*-fundamental and the SF waves: $\Delta k'_{br_o}=0$ and no group velocity dispersion. In Fig. 4(a), the propagation is stopped at the location where the two fundamental pulses meet, and it is evident that the phase profile of $B(t)$ differs from the phase of $R_o(t)$. Actually, the phase profile of $B(t)$ is equal to the phase profile of the *o*-wave only in the right part of $R_o(t)$, i.e., in the part that has already experienced a complete interaction with the *e*-fundamental wave. Moreover, since the mixing process is not complete, the SF pulse is delayed relative to the *o*-pulse even if the two pulses travel at the same group velocity. Fig. 4(b) shows the same amplitudes and phases but at the output of the crystal ($L=2t_0/\Delta k'_{r_e r_o}$). Now, the complex amplitude of $R_o(t)$ has been entirely transferred to the SF wave $B(t)$. This example shows that a waveform transfer from the fundamental wave to the SF wave is possible only if the pulse R_e walks completely through R_o in the nonlinear crystal. This requirement imposes an upper limit on the time support ΔT allowing an accurate replication of the pulse.

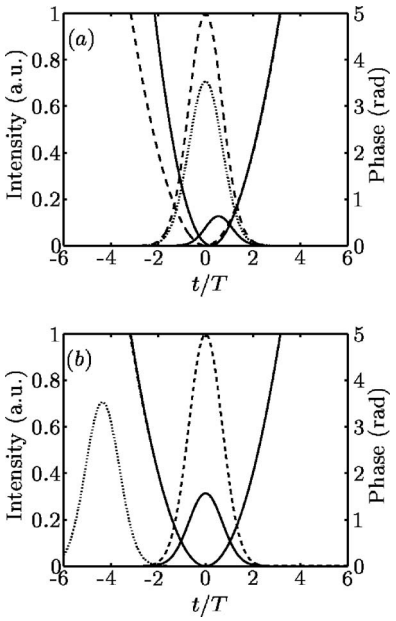

Fig. 4. Evolution of the amplitude and the phase of $B(t)$, with $\Delta k'_{br_o}=0$ and $t_0=4.3T$. Amplitude and phase of R_o (dashed curves), amplitude and phase of B (solid curve) and amplitude of R_e (dotted curve), (a) in the crystal at the location where the two fundamental pulses meet, (b) at the output of the crystal where they have walked through each other.

In the spectral region where the group velocities of the *o*-fundamental and the SF pulses do not match (i.e., $\Delta k'_{br_o}\neq 0$), we have seen that the SF pulse replicates the fundamental *o*-pulse up to a known time axis scaling factor s [see Fig. 8(a)] and a known time shift Δt that depends only on the crystal properties. The latter does not exceed 15% of the predelay t_0 for a KDP crystal in the spectral range between 750 and 900 nm. This result is illustrated in Fig. 5 for a group velocity mismatch $\Delta k'_{br_o}=0.15\Delta k'_{br_e}$ (as for a KDP crystal of ~750 nm). The dashed curves show the intensity and the phase profile of the SF pulse at the output of the crystal, and it can be seen that if the SF pulse is stretched by the calculated factor $s=0.85$ and delayed by $L\Delta k'_{br_o}+\Delta t=0.645T$, the complex amplitude of the SF pulse (circles) is a perfect replica of the *o*-fundamental pulse (solid curves).

B. Effect of Group Velocity Dispersion

In dispersive materials, the transfer function relation in Eq. (14) is no longer accurate because it neglects the GVD at both fundamental and SF frequencies. However, to the first order, the GVD can straightforwardly be taken into account, since it leads to an extra phase $\Delta\varphi=1/2k''_{\text{eff}}L\omega^2$, which can be derived as follows: Assuming the SF pulse is generated in the crystal at the location l where the two fundamental pulses meet

$$l = t_0/\Delta k'_{r_e r_o}, \quad (19)$$

the effective GVD can be split into two terms:

$$k''_{\text{eff}}L = k''_{r_o} l \times \frac{1}{s^2} + k''_b (L-l). \quad (20)$$

The first term of the right-hand side of Eq. (20) accounts for the chirp acquired by the *o*-pulse while traveling in the crystal to the location l. The factor $1/s^2$ has been added because of the temporal scaling factor that appears in Eq. (14). The second term describes the chirp acquired by the SF pulse from the location l to the end of the crystal. Therefore the frequency representation of the SF

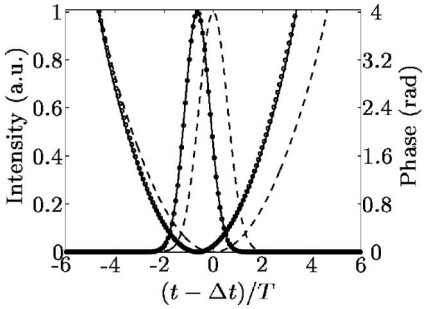

Fig. 5. SF generation in presence of a a group velocity mismatch ($\Delta k'_{br_o}=0.15\Delta k'_{br_e}$). Intensity and phase profiles of the SF pulse (dashed curves) and the *o*-fundamental pulse (solid curves) at the output of the crystal. The initial conditions are identical as for Fig. 4. The shifted and scaled output SF pulse is also shown (circles).

pulse at the output of the crystal can be approximated by combining the results in Eqs. (14) and (20), and taking into account the frequency shift ($\Delta\omega$) from the carrier frequency of the SF pulse,

$$\tilde{B}(\omega,L) \approx \tilde{B}_0(\omega,L)\exp\left(\frac{i}{2}k''_{\text{eff}}L(\omega-\Delta\omega)^2\right), \qquad (21)$$

where $\tilde{B}_0(\omega,L)$ is the frequency representation of the temporal signal in Eq. (14). The accuracy of the last expression has been verified by comparing Eq. (21) with the numerical simulation of the system in Eq. (5). A typical example is shown in Fig. 6 for a pulse with a complex temporal shape resulting from a Gaussian spectrum centered at ~760 nm (14.5 nm bandwidth FWHM) with quadratic and cubic spectral phase components (200 fs^2 and 3×10^4 fs^3, respectively). The optical properties of KDP crystal cut for type II second harmonic generation at 760 nm have been used to calculate the group velocity mismatch $\Delta k'_{br_o} = 0.117\Delta k'_{br_e}$. The length of the crystal has been set to 10 mm and the predelay t_0 to 600 fs. Eventually, the angle of propagation has been tilted by 4 mrad (0.23°) from the phase-matching angle for second harmonic generation at 760 nm resulting in a frequency shift $\Delta\omega = 4.1$ mrad fs^{-1}. The solid curves in Fig. 6 show the amplitude and the phase of the SF pulse at the output of the crystal obtained by numerically solving the system (5). Dots correspond to the amplitude and the phase given by our model in Eq. (21). As can be seen, the agreement between the numerical solution and our model is very good although the GVD was taken into account only in the first order approximation.

The most important feature of Eq. (21) is that the SF pulse is linked to the input pulse by a simple linear transformation that does not depend on the shape of the input pulse but only on the physical properties of the nonlinear crystal used. This is essential if we want to implement a spectral shearing interferometer based on the SF generation process described above.

4. PULSE MEASUREMENT

ARAIGNEE is a technique for the characterization of the electric field of ultrashort optical pulses based on spectral shearing interferometry. It relies on the spectral interferogram generated by a pair of temporally delayed and spectrally shifted replicas of the test pulse. In ARAIGNEE, the spectral shear Ω is the result of a slight tilt between the two beams in the nonlinear crystal.

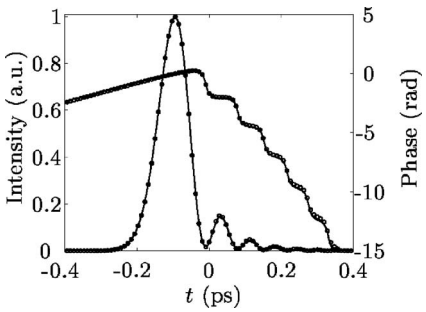

Fig. 6. Comparison of the amplitude and the phase of the SF pulse at the output of a thick KDP crystal obtained by numerically solving the system (5) (solid curves) and derived from Eq. (21) (circles).

From Eq. (21), the spectral interferogram $\tilde{S}(\omega)$ of the two SF pulses is given by

$$\begin{aligned}\tilde{S}(\omega) &= |\tilde{B}_1(\omega) + \tilde{B}_2(\omega-\Omega)\exp(-i\omega\tau)|^2 \\ &= |\tilde{B}_1(\omega)|^2 + |\tilde{B}_2(\omega-\Omega)|^2 + 2|\tilde{B}_1(\omega)||\tilde{B}_2(\omega-\Omega)| \\ &\quad\times\cos\left[\phi_0\left(\frac{\omega}{s}\right) - \phi_0\left(\frac{\omega-\Omega}{s}\right) + \delta\phi(\omega) + \omega\tau\right],\end{aligned} \qquad (22)$$

where the subscripts (1, 2) distinguish the two SF pulses, $\phi_0(\omega)$ is the spectral phase of the test pulse, which is the information we wish to recover, and $\Omega = \Delta\omega_1 - \Delta\omega_2$ is the spectral shear.

$\tilde{S}(\omega)$ has a form of a standard shearing interferogram consisting of fringes nominally spaced in frequency at $2\pi/\tau$, while the phase difference term $\phi_0(\omega/s) - \phi_0([\omega - \Omega]/s) + \delta\phi(\omega)$ manifests itself as a deviation from the nominal fringe spacing. Since the two SF pulses travel at a different group velocity in the crystal, the time delay τ is not the delay between these two pulses at the output of the crystal but must be interpreted as the delay between the pair of *e*- (or *o*-) polarized pulses before the crystal. The additional time delay resulting from the birefringence, as well as the chromatic dispersion is included in the term $\delta\phi(\omega)$ defined as

$$\delta\phi(\omega) = (\Delta t_1 - \Delta t_2 + \Omega k''_{\text{eff}}L)\omega, \qquad (23)$$

where the two first terms are defined by Eq. (18) and depend on the actual angle of propagation of the two beams. The effective GVD is given by Eq. (20) and is assumed to be identical for both beams.

The phase difference between the two SF pulses is extracted by Fourier transforming the interferogram, filtering the peak around the pseudotime $+\tau$ and inverse Fourier transforming to the frequency domain.

As for a standard SPIDER interferogram, it can be seen from Eq. (22) that knowledge of the shear and the reference phase $\omega\tau + \delta\phi(\omega)$ is essential for recovering the spectral phase ϕ_0 [7]. In the experiment, the shear can simply be measured from the two individually recorded upconverted spectra. The reference phase is usually obtained by recording an additional spectrogram without spectral shear. In ARAIGNEE, zeroing the shear means canceling the angular tilt between the two beams and this cannot be done without changing the delay between the pulses. As a result, the reference phase cannot be recorded at the SF frequencies. However, the reference phase can be extracted from the interferogram between the pair of fundamental *e*- or *o*-pulses at the output of the crystal. Extracting the reference phase from the interferogram with the same polarization state as the SF pulses enables us to minimize the spatial walk-off between the reference and the SF beams. The experimental procedure therefore requires no intermediate alignment and the fundamental and SF interferogram can be recorded either simultaneously [17] or separately [7]. For instance, in KDP crystal the phase-matching as well as the group velocity

matching requirements are fulfilled for "oee" interaction at approximately 830 nm, and the reference phase is extracted from the phase difference $\omega\tau+(\Delta k'^{2}_{br_e}-\Delta k'^{1}_{br_e})L\omega$ between the two fundamental e-pulses.

The linear phase extracted from calibration is subtracted from the phase difference between the two SF pulses to give the phase difference $\phi_0(\omega/s)-\phi_0([\omega-\Omega]/s)$ minus a linear phase correction $\delta\phi_{\text{corr}}(\omega)=[\Delta t_2-\Delta t_1+(\Delta k'^{2}_{br_e}-\Delta k'^{1}_{br_e}-k''_{\text{eff}}\Omega)L]\omega$ that depends only on the geometry of the apparatus and the optical properties of the crystal. The correction term can be removed either before or after the standard concatenation algorithm used to reconstruct $\phi(\omega/s)$ from the phase difference [7,18]. After concatenation the correction function $\phi_{\text{corr}}(\omega)$ appears as a quadratic phase. Indeed, if the integration approximation is used, then

$$\phi_{\text{corr}} \approx \frac{1}{\Omega}\int \delta\phi_{\text{corr}}(\omega)\mathrm{d}\omega = a_{\text{corr}}\omega^2, \tag{24}$$

with

$$a_{\text{corr}} = \frac{1}{2\Omega}[(\Delta k'^{2}_{br_e} - \Delta k'^{1}_{br_e})L + \Delta t_2 - \Delta t_1] - \frac{1}{2}k''_{\text{eff}}L. \tag{25}$$

It is better to apply the phase correction after the concatenation because, although $\delta\phi_{\text{corr}}$ varies with the shear, a_{corr} is independent of the shear, that is of the exact beam propagation angles, but depends only on the crystal dispersion, its length L, and the predelay t_0. A numerical evaluation of Eq. (25) has shown that a_{corr} does not vary more than 0.1% up to a shear of 40 mrad fs^{-1} (3.6 nm at $\lambda=415$ nm). After frequency scaling by the factor s, the resulting phase profile is the spectral phase profile of the unknown pulse. However, if the predelay is the result of the propagation of the pulse through a birefringent medium, the added spectral phase associated with the medium dispersion must be subtracted. Finally, a measurement of the spectral density completes the pulse characterization. The block diagram in Fig. 7 summarizes the phase retrieval procedure. The wavelength dependence of the scaling factor s for KDP crystal as well as the quadratic phase factor a_{corr} for a crystal length of 5 mm and a predelay $t_0=317$ fs, as used in our setup presented in Fig. 2 are plotted in Fig. 8.

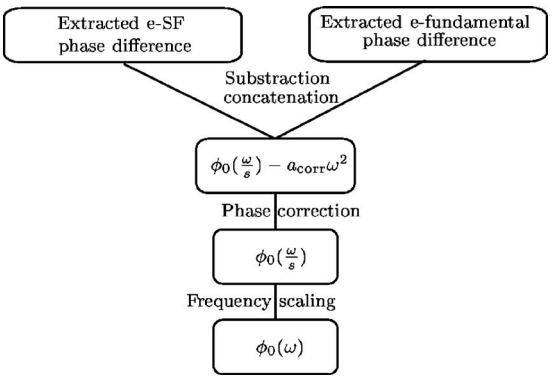

Fig. 7. Block diagram of the phase retrieval procedure in ARAIGNEE.

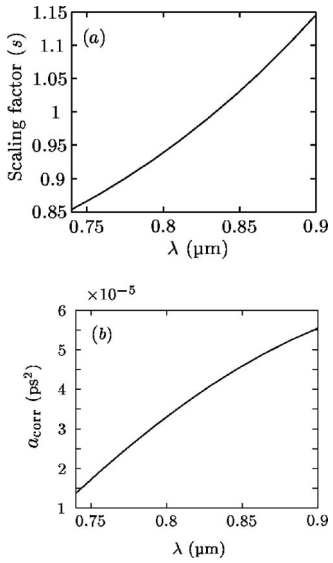

Fig. 8. Scaling factor s (a) and quadratic phase factor a_{corr} (b) as a function of the central wavelength of the unknown pulse for KDP. The parameters used in (b) are: crystal thickness $L=5$ mm, predelay $t_0=317$ fs.

5. EXPERIMENTAL CONSIDERATIONS

Figure 2 displays the schematic of a compact ARAIGNEE setup. The linearly polarized input pulse passes through a zero-order $\lambda/2$-wave plate and a crystalline quartz plate (10 mm thick, slow axis horizontal), the two elements splitting it into ordinary and extraordinary polarizations, with the e-wave being predelayed by 317 fs with respect to the o-wave. The beam is subsequently sent onto a pair of mirrors adjacent to each other with a small mutual horizontal tilt β that splits the incident beam into two beams [19] (see detail in Fig. 2). The two beams are directed into a 5 mm thick KDP crystal, cut for second harmonic generation at 830 nm and oriented such that the optic axis is horizontal. Each beam undergoes type II SF generation and the resulting SF pulses are spectrally shifted (sheared) due to the angular offset (2β) of the fundamental beams in the crystal. In our experiment, the angle β has been set to 0.25° resulting in a spectral shear of ~0.8 nm, i.e., 10% of the pulse bandwidth [20]. The mirror tilt direction (beams diverging) has been chosen to make selecting individual beams for shear measurement easier. The opposite configuration (beams converging) eliminates the need for imaging optics [8], and decreases the gap between the two mirrors. A longitudinal shift of one of the two mirrors by $d\simeq 225$ μm delays the corresponding pulse by $\simeq$1.5 ps as required by spectral interferometry. The stability of the mechanics for d and β is an important feature but does not need to have a precisely calibrated scale. At the output of the crystal, the two beams are recombined with a 100 mm focusing mirror onto the entrance slit of a compact grating spectrometer (USB2000, Ocean Optics). The diameter of the input beam must be larger than ~2 mm to minimize the effect of the gap between the two mirrors in the pair, the diffraction of the edges as well as the spatial walk-off in the crystal (of the order of 20 mrad [21]). On the other hand, the wave plate and the KDP crystal used (10×10 mm) limit the maximum device aperture to approximately

5 mm. Another implementation of ARAIGNEE has been proposed in which the two angularly tilted and temporally delayed beams are generated by a Michelson interferometer arrangement [6]. The lower limit of the beam diameter is therefore only imposed by the spatial walk-off in the crystal.

The calibration in ARAIGNEE is based on the retrieval of the spectral phase from an interferogram between two *e*-polarized test pulses (see Fig. 7). In our ARAIGNEE setup, this interferogram is generated by rotating the λ/2-wave plate in such a way that the polarization direction of the beam matches the horizontal axes of both the quartz and the KDP crystal. Finally, the spectral phase accumulated by the pulses by propagating through the 10 mm quartz plate (196 fs^2 at 830 nm) is removed after the frequency scaling.

We used several sources of ultrashort pulses to characterize the performances of our ARAIGNEE device: a MaiTai (Spectra-Physics) laser delivering ≃70 fs pulses centered in the 750–850 nm range, a Mira Seed (Coherent) providing broader bandwidth pulses (Δλ≃30 nm) and a 1 kHz chirped pulse amplifier (CPA). The dashed curves plotted in the left part of Fig. 9 show the spectral phase reconstruction of the MaiTai laser pulses of different central frequency. The comparison with the spectral phase measured with a conventional SPIDER apparatus [7] (solid curves) shows an excellent agreement between the ARAIGNEE and the SPIDER measurements. These results demonstrate that the spectral phase of an ultrashort pulse can be measured with ARAIGNEE outside the spectral range where a perfect group velocity matching occurs as predicted by our theoretical analysis, providing that the scaling factor in Eq. (15) is taken into account. Note that since the sensitivity of ARAIGNEE is higher than SPIDER, the average power of the laser beam was attenuated down to 25 mW average (0.3 nJ/pulse) in the former case, that is 1 order of magnitude lower than with our conventional SPIDER apparatus. This is the result of a longer interaction length for the sum-frequency generation and no chirped ancillary pulse.

As an additional consistency check of the ARAIGNEE method, we performed the measurement of the spectral phase added to the MaiTai laser pulses after propagation through various lengths of the BK7 glass from 10 to 100 mm. The accumulated quadratic spectral phase has been compared with the theoretical curve calculated from the Sellmeier equation. The very good agreement between the reconstructed phase by ARAIGNEE and the theoretical profile [5] demonstrates the reliability of the ARAIGNEE device. Particularly, this result shows that the spectral chirp of the *e*-polarized fundamental pulse does not affect the arrival time of the SF pulse at the output of the crystal, or, in other words, the delay between the two spectrally sheared SF pulses. We performed the same experiment with 30 fs pulses (FWHM) from the Mira Seed laser. The reconstructed spectral phase plotted in Fig. 10(a) has a positive curvature of 220 fs^2, which agree very well with the 200 fs^2 calculated from the Sellmeier equation.

We also tested ARAIGNEE for structured pulses. The spectral phase of the Gaussian pulses generated by a CPA laser system was sinusoidally modulated by a pulse shaper consisting of a programable acousto-optic modulator (AOM) placed in the focal plane of a 4-*F* grating-and-lens apparatus [22]. The spectral phase retrieved from the measurement with the Michelson arrangement of ARAIGNEE [6] was compared with conventional SPIDER results. As can be seen in Fig. 10(b) both measurements

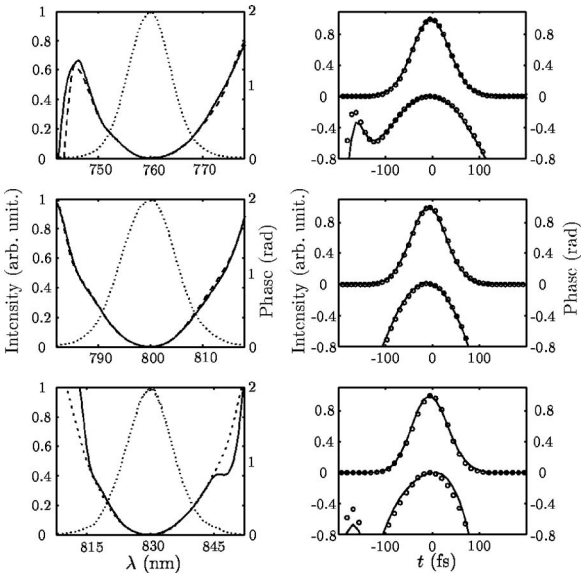

Fig. 9. Left: Spectrum of the test pulse (dotted curve) and its spectral phase retrieved by ARAIGNEE (dashed curve) and SPIDER (solid curve) for various central wavelengths. Right: Time-dependent intensity and phase measured by ARAIGNEE (circles) and SPIDER (solid curve) from the data plotted on the left.

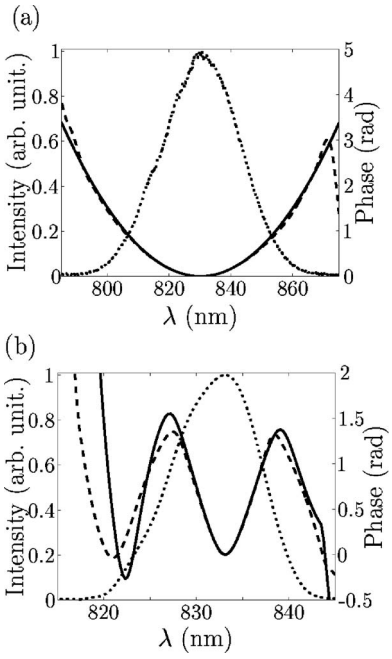

Fig. 10. (a) Spectrum of the Mira Seed laser (dotted curve) and acquired spectral phase after propagation through 9.5 mm of BK7 (dashed curve). The solid curve shows the fit to the phase that corresponds to a group delay dispersion of 440 fs^2. (b) Spectral intensity of the test pulse (dotted curve) and sinusoidal modulation of its spectral phase reconstructed by ARAIGNEE (dotted curve) and SPIDER (solid curve).

agree perfectly over the central part of the spectrum with some discrepancies in the wings. The low signal level at the output of the pulse shaper is responsible for the SPIDER phase deviating somewhat from the sinusoidal profile while the more sensitive ARAIGNEE recovers this profile with higher accuracy.

6. DISCUSSION

The condition of complete walkthrough of the two fundamental test pulses in the nonlinear crystal results in a limitation of the time support ΔT for an accurate measurement of the test pulse. On the other hand, the maximum bandwidth of the pulse is limited by the GVD. Indeed, the GVD leads to the distortion of the test pulses that, in turn, affects both the amplitude and the phase of the SF pulse. This effect is proportional to the magnitude of the GVD, the pulse bandwidth and the interaction length. In the PMF picture, the GVD manifests itself as a curvature of the PMF (see Fig. 1). The amplitude distortion can be qualitatively understood from this figure: the frequencies in the wings of the *o*-pulse are mixed with a lower frequency of the *e*-pulse than the *o*-pulse carrier frequency.

To quantify the consequences of both the GVD and the group velocity mismatch $\Delta k'_{br_o}$ on the accuracy of the ARAIGNEE method, we have numerically simulated the generation of the two spectrally sheared replica and applied our reconstruction algorithm. The rms error ε between the input and the reconstructed electric fields, respectively, E_{in} and E_{rec}, defined as

$$\varepsilon = \|E_{\text{in}}(t) - E_{\text{rec}}(t)\|, \tag{26}$$

where the norm of the field is $\|E\| = [\int_{-\infty}^{\infty} |E(t)|^2 \mathrm{d}t]^{1/2}$ and where the two complex amplitudes are normalized to unity, has been used to quantify the reconstruction error [18].

In Fig. 11(a) we have plotted the rms error ε for a transform-limited Gaussian input pulse at different central wavelengths and of different bandwidths, for an ARAIGNEE apparatus with a 20 mm nonlinear KDP crystal (with a predelay $t_0 = 1440$ fs such that the *o*- and the *e*-pulses meet halfway in the crystal). Following [18], we consider the reconstruction very good for ε below 0.02, average for ε between 0.02 and 0.1 and poor for ε exceeding 0.1. A qualitative understanding of the metric used is provided by Figs. 11(b) and 11(c). A single KDP crystal (20 mm thick) can be used to measure pulses from 60 to 700 fs in the spectral range from 0.74 to 0.9 μm with the restrictive criterion $\varepsilon < 0.02$. The result plotted in Fig. 11(a) also shows that the rms error is minimal near 830 nm. The increase of the rms error away from that region comes from the terms we have neglected in Eq. (12). Indeed, for such wavelengths, the assumption that $\Delta k'_{br_o}/\Delta k'_{br_e} \ll 1$ is no longer valid and the higher order terms lead to a distortion of the SF pulse from a perfect replica of the input pulse. The performance of ARAIGNEE has also been studied for complex pulses. As an example, the reconstruction of two 50 fs transform-limited Gaussian pulses, separated by 0.2 ps and centered ~800 nm, is shown in Fig. 12. As can be seen, the two pulses are very well retrieved in spite of the fact that

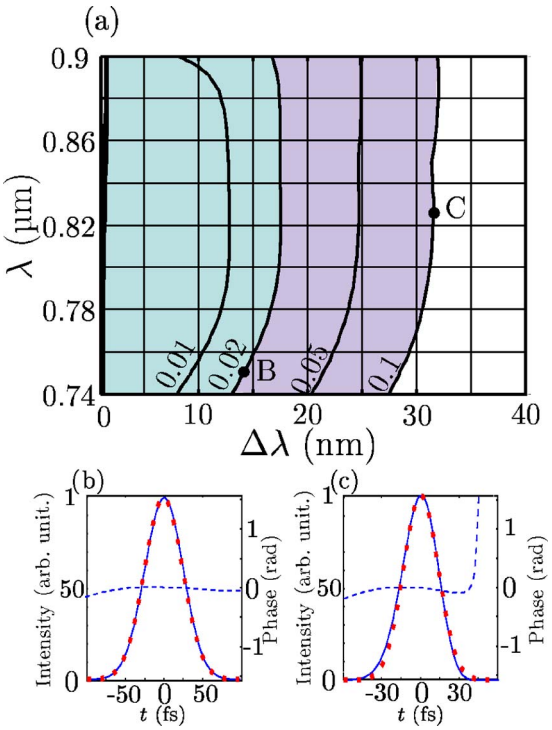

Fig. 11. (Color online) (a) rms error ε of the retrieved pulse calculated from numerical simulation of the SF generation in a 20 mm thick KDP crystal as a function of the input pulse bandwidth (intensity FWHM) and central wavelength for Gaussian transform-limited input pulses. (b), (c) Temporal intensity profile (dotted curves) of the test pulse corresponding to B and C in (a) and reconstructed intensity (solid curves) and phase (dashed curves) profiles.

each pulse in the *e*-polarized pair takes part in the SF generation. The small residual phase leads to a rms error as low as 0.03.

Pulses in other wavelength ranges can also be characterized by ARAIGNEE providing that a suitable nonlinear crystal is chosen. In Fig. 13 we have plotted the spectral range of tunability for two commonly used nonlinear crystals: BBO and KTP. With a KTP crystal in the YZ plane ($\phi = 90°$), both the group velocity matching and the phase-matching are achieved at a wavelength of 1422 nm, for the "oeo" interaction at an angle $\theta = 47°$. With our conservative requirement of $\varepsilon < 0.02$, a 20 mm thick crystal allows the measurement of pulses in the telecom band in the range of ~60–900 fs FWHM. In addition, the PM function of an oee interaction in a BBO crystal is vertical

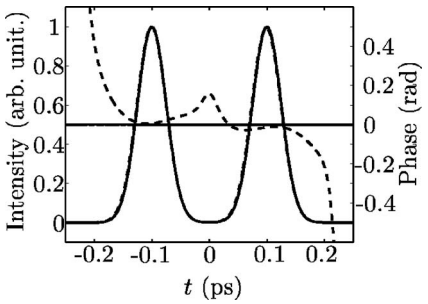

Fig. 12. Simulated reconstruction of a double Gaussian pulse at 800 nm (dashed curve). The solid curves show the test pulse intensity and phase.

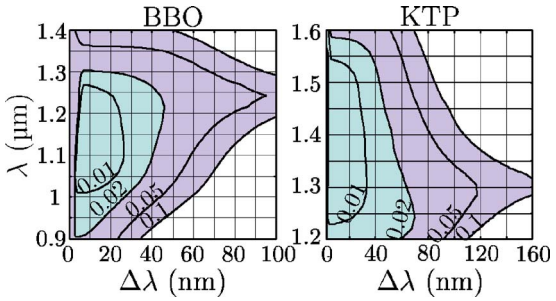

Fig. 13. (Color online) Simulated rms error ε of an ARAIGNEE device with a 20 mm thick BBO and KTP in the YZ plane, and a quartz plate 40 and 50 mm thick, respectively.

at a wavelength of 1169 nm (θ=31°). This crystal is therefore suitable to measure pulses in the range 1.0–1.3 μm where new, powerful, diode-pumped mode-locked lasers based on Yb-doped materials become available. The rms error of very short pulses is no longer minimal around the group velocity matching wavelength but ~1.3 μm instead where the GVD experienced by the pulse in the quartz plate prior to propagating in the nonlinear crystal is minimal. Table 1 enables us to quickly find the proper crystal type and length for a given application. It displays the maximum bandwidth allowing very good or average reconstruction of transform-limited Gaussian pulses. The predelay is assumed to be the result of the propagation through a quartz plate with the appropriate length.

The full characterization of the electric field of an optical pulse both in space and time is an active research area in optical metrology since space-time coupling occurs in the manipulation of light as simple as focusing as well as in most nonlinear interactions. Recently, the SEA-SPIDER (spatial encoding for SPIDER) method where the spectral phase is encoded in the spatial fringes between two spectrally sheared replicas has been developed to measure extremely short pulses [10,11]. Since a two-dimensional sensor is used to record the fringes, this method naturally measures the spatial dependence of the pulse along one transverse coordinate. Similarly, the spatial encoding method can straightforwardly be applied to ARAIGNEE by combining a Michelson interferometer to split the beam in two parts, with an imaging spectrometer. Note that in the splitting mirror implementation of ARAIGNEE as depicted in Fig. 2, a reliable measurement of the pulse can still be performed in the presence of space–time coupling as long as it involves only a spatial variation of the central frequency within the beam, since we have direct access to the spectral shear.

ARAIGNEE is based on the general principle of a group velocity mismatch between two fundamental test pulses as well as a group velocity match between the SF pulse and one of the two test pulses. Therefore quasi-phase-matched crystals can be designed to achieve the phase-matching at a desired wavelength where the group velocity requirements are already satisfied. Moreover, when an external powerful optical beam is available, it can be used as a source of the fundamental pulse with the group velocity mismatch, similarly to the modified SPIDER proposed to improve the sensitivity of the spectral shearing interferometry [23].

7. SUMMARY

ARAIGNEE (another ridiculous acronym for interferometric geometrically simplified noniterative *E*-field extraction) is a novel implementation of spectral shearing interferometry for measuring ultrashort pulses. It takes advantage of the properties of sum-frequency (SF) generation in a type II nonlinear crystal to dramatically simplify the generation of the sheared replicas. Indeed, it is the phase-matching function itself that selects the single frequency to be upconverted with the test pulse, eliminating the requirement for linearly chirped ancillary pulses and the components that produced them. Moreover, due to the intrinsic collinear geometry, the pulses automatically overlap both spatially and temporally in the crystal, offering a user-friendly apparatus. ARAIGNEE is also more sensitive than a conventional SPIDER since the crystal used is longer.

Table 1. Maximum Pulse Bandwidth (Δλ) That Can Be Measured with an rms Error Less than 0.02 or 0.1

Crystal	L (mm)	t_0 (fs)	Δλ (nm) $\epsilon<0.02$		Δλ (nm) $\epsilon<0.1$	
			λ=750 nm	λ=830 nm	λ=750 nm	λ=830 nm
KDP	20	1450	14	17	28	32
oee	5	360	23	25	46	49
	1	75	—	—	77	77
			λ=1000 nm	λ=1169 nm	λ=1000 nm	λ=1169 nm
BBO	20	1100	39	42	88	89
oee	5	275	49	49	103	130
	1	55	—	—	165	204
			λ=1422 nm	λ=1550 nm	λ=1422 nm	λ=1550 nm
KTP_YZ	20	1750	49	30	98	70
oeo	5	440	60	46	155	120
	1	85	—	—	246	197

We have presented a comprehensive description of the SF generation in the nonlinear crystal. Our analytical model shows that a wide range of pulse lengths and central wavelengths can be accurately characterized by ARAIGNEE, but the device calibration requires a reasonable knowledge of the crystal properties. The capabilities of ARAIGNEE have been experimentally demonstrated for pulses of various bandwidths, central wavelengths, and spectral phases. As with other spectral shearing interferometric techniques, ARAIGNEE requires only 1D data collection for pulse reconstruction, has a fast inversion algorithm as well as one shot capabilities. ARAIGNEE can also be used in other SPIDER schemes such as modified-SPIDER [23] or SEA-SPIDER [10,11] for increased sensitivity or space–time coupling measurements, respectively.

ACKNOWLEDGMENTS

This work was supported by the Engineering and Physical Sciences Research Council, grant EP/D503248/1. S.-P. Gorza acknowledges the support of the Wiener-Anspach Foundation and the Fonds National de la Recherche Scientifique (FRS-FNRS, Belgium) and A. Radunsky acknowledges the support of the National Science Foundation.

REFERENCES

1. V. Wong and I. A. Walmsley, "Linear filter analysis of methods for ultrashort-pulse-shape measurements," J. Opt. Soc. Am. B **12**, 1491–1499 (1995).
2. C. Radzewicz, P. Wasylczyk, and J. S. Krasiński, "A poor man's FROG," Opt. Commun. **186**, 329–333 (2000).
3. P. O'Shea, M. Kimmel, X. Gu, and R. Trebino, "Highly simplified device for ultrashort-pulse measurement," Opt. Lett. **26**, 932–934 (2001).
4. D. T. Reid and I. G. Cormack, "Single-shot sonogram: a real-time chirp monitor for ultrafast oscillators," Opt. Lett. **27**, 658–660 (2002).
5. A. S. Radunsky, I. A. Walmsley, S. P. Gorza, and P. Wasylczyk, "Compact spectral shearing interferometer for ultrashort pulse characterization," Opt. Lett. **32**, 181–183 (2007).
6. A. S. Radunsky, E. M. Kosik, I. A. Walmsley, P. Wasylczyk, W. Wasilewski, A. B. U'Ren, and M. E. Anderson, "Simplified spectral phase interferometry for direct electric-field reconstruction by using a thick nonlinear crystal," Opt. Lett. **31**, 1008–1010 (2006).
7. C. Iaconis and I. A. Walmsley, "Self-referencing spectral interferometry for measuring ultrashort optical pulses," IEEE J. Quantum Electron. **35**, 501–509 (1999).
8. A. Monmayrant, S.-P. Gorza, P. Wasylczyk, and I. Walmsley, "Beyond the fringe: SPIDER—the anatomy of ultrashort laser pulses," Photon. Int. 44 (2007).
9. P. Baum, S. Lochbrunner, and E. Riedle, "Zero-additional-phase SPIDER: full characterization of visible and sub-20-fs ultraviolet pulses," Opt. Lett. **29**, 210–212 (2004).
10. E. M. Kosik, A. S. Radunsky, I. A. Walmsley, and C. Dorrer, "Interferometric technique for measuring broadband ultrashort pulses at the sampling limit," Opt. Lett. **30**, 326–328 (2005).
11. A. S. Wyatt, I. A. Walmsley, G. Stibenz, and G. Steinmeyer, "Sub-10 fs pulse characterization using spatially encoded arrangement for spectral phase interferometry for direct electric field reconstruction," Opt. Lett. **31**, 1914–1916 (2006).
12. A. P. Baronavski, H. D. Ladouceur, and J. K. Shaw, "Analysis of cross correlation, phase velocity mismatch, and group velocity mismatches in sum-frequency generation," IEEE J. Quantum Electron. **29**, 580–589 (1993).
13. R. W. Boyd, *Nonlinear Optics*, 2nd ed. (Academic, 2003).
14. H. Wang and A. M. Weiner, "A femtosecond waveform transfer technique using type II second harmonic generation," IEEE J. Quantum Electron. **40**, 937–945 (2004).
15. W. P. Grice, A. B. U'Ren, and I. A. Walmsley, "Eliminating frequency and space-time correlations in multiphoton states," Phys. Rev. A **64**, 063815 (2001).
16. E. Sidick, A. Knoesen, and A. Dienes, "Ultrashort-pulse second-harmonic generation. I. Transform-limited fundamental pulses," J. Opt. Soc. Am. B **12**, 1704–1712 (1995).
17. C. Dorrer, "Implementation of spectral phase interferometry for direct electric-field reconstruction with a simultaneously recorded reference interferogram," Opt. Lett. **24**, 1532–1534 (1999).
18. C. Dorrer and I. A. Walmsley, "Accuracy criterion for ultrashort pulse characterization techniques: application to spectral phase interferometry for direct electric field reconstruction," J. Opt. Soc. Am. B **19**, 1019–1029 (2002).
19. I. Z. Kozma, P. Baum, U. Schmidhammer, S. Lochbrunner, and E. Riedle, "Compact autocorrelator for the online measurement of tunable 10 femtosecond pulses," Rev. Sci. Instrum. **75**, 2323–2327 (2004).
20. M. E. Anderson, L. E. E. de Araujo, E. M. Kosik, and I. A. Walmsley, "The effect of noise on ultrashort-optical-pulse measurement using SPIDER," Appl. Phys. B **70**, S85–S93 (2000).
21. V. G. Dimitrev, G. G. Gurzadyan, and D. N. Nikogosyan, *Handbook of Nonlinear Optical Crystals*, 2nd ed. (Springer-Verlag, 1997).
22. C. W. Hillegas, J. X. Tull, D. Goswami, D. Strickland, and W. S. Warren, "Femtosecond laser pulse shaping by use of microsecond radio-frequency pulses," Opt. Lett. **19**, 737–739 (1994).
23. M. Hirasawa, N. Nakagawa, K. Yamamoto, R. Morita, H. Shigekawa, and M. Yamashita, "Sensitivity improvement of spectral phase interferometry for direct electric-field reconstruction for the characterization of low-intensity femtosecond pulses," Appl. Phys. B **74**, S225–S229 (2002).